Partial 1420 MHz HI Survey of the North Polar Spur

Aaron Tran[1,3]
Isaac A. Domagalski[1,2], Caleb Levy[1,2]
Aaron Parsons[2,4,5], Garrett K. Keating[2,4,5], Baylee Bordwell[2,5]
[1]Central Intelligence Agency, 1000 Colonial Farm Rd, McLean, VA 22101, USA
[2]Dept. Astronomy, UC Berkeley, D-23 Hearst Field Annex, Berkeley, CA 94720, USA
[3]Dept. Earth and Planetary Science, UC Berkeley, 335 McCone Hall, Berkeley, CA 94720, USA
[4]Radio Astronomy Laboratory, UC Berkeley, Berkeley, CA 94720, USA
[5]Undergraduate Radio Laboratory teaching staff
Received in incomplete form 2014 May 6, revised in incomplete form 2014 May 8

Abstract

We observe the north polar spur and make a nice picture. We can make out a spur in column density, and I speculate that a northerly ridge is visible in velocity dispersion.

1 Introduction

The North Polar Spur is a prominent ridge structure within a larger bubble-like structure above the plane of the Milky Way (positive galactic latitude, $b > 0$) known as the Loop-I region [*Heiles et al.*, 1980]. The shell(s?) bounding the Loop-I region and giving rise to the North Polar Spur are thought (weasel word: by whom?) to be propelled by supernovae shocks and stellar winds from the Sco-Oph (Sco-Cen?) OB association of stars. Swept-up interstellar HI gas emits in radio and X-ray wavelengths due to 21 cm and synchrotron emission. Synchrotron emission might trace energetic physical processes or magnetic fields in the Loop-I shells. Here we investigate HI line emission, which allows us to probe (1) shell column densities, and (2) velocities of the bulk gas.

1.1 The HI 21 cm line

The 1420 MHz line arises from a forbidden hyperfine transition in neutral hydrogen (HI) gas. The hyperfine transition arises due to spin-spin ($\vec{S} \cdot \vec{I}$) coupling between the hydrogen proton and electron, which splits the ground ($1s$) state into two levels with frequency separation 1420.40575 MHz [e.g. *Wittke and Dicke*, 1956; *Kleppner, Goldenberg, and Ramsey*, 1962] (these references are kind of old, couldn't find a newer source for the most accurate line measurement).

Although the HI line transition is quantum mechanically forbidden (angular momentum selection rules), the low transition rate and low (radio) wavelength implies that hyperfine emission of HI easily reaches thermal equilibrium. Therefore, HI line emission should directly reflect source temperatures and densities.

Some comments about physical significance of neutral HI in the galaxy go here?

Here's a simple equation for column density:

$$\eta_H \approx (1.82 \times 10^{18}\ \mathrm{K^{-1} km^{-1} s}) \int T_b\,(v)\,dv$$

where η_H is column density in units of cm^{-2} and $T_b(v)$ is brightness temperature (K) as a function of velocity (km/s) [*Condon and Ransom*, 2006].

1.2 Questions that can be addressed

Here I should discuss a bit more about shock-ISM interaction if there is time (partially out of own interest). Karto mentioned a lot of interesting physical processes that might be discussed – by discuss, I mean at least think about whether they are visible or may be probed at all. In particular, shell shape (thickness,

density, velocity) may tell us something about the interstellar medium distribution around the Milky Way, the history of the shell (what energy is needed to mobilize some amount of gas?), et cetera. This would require myriad assumptions and guesses.

2 Observations

2.1 Leuschner radio dish

We use the Leuschner radio dish (37°55′10.2″ N, −122°09′12.4″ E), operated by UC Berkeley as part of Leuschner Observatory, to collect single-dish observations of the hyperfine HI line. The Leuschner radio dish, hereafter Leuschner (Figure 1), has diameter 3.6 m or 4.5 m depending on who is asked; the beamwidth is $\sim 4°$ at its operating frequency of 1420 MHz. Leuschner's view at low altitudes is blocked by surrounding hills; to the north Leuschner may point above $\sim 50°$, to the south Leuschner may point to 20–30° altitude. The Leuschner radio dish was originally built for the SETI Rapid Prototype Array near Leuschner Observatory, an early prototype for the now-underfunded and incomplete Allen Telescope Array. The dish has since been appropriated for undergraduate education; its sibling dishes have been dismantled or turned into gigantic bats (e.g., http://patriciavader.com/artwork/1696610_The_Giant_Bat.html).

Figure 1. The Leuschner dish has beamwidth $\sim 4°$ at 1420 MHz. Here the dish is shown with its erstwhile caretaker, *kartp* (courtesy of I. Domagalski, E. Herrera, K. Moses).

RF waves incident on Leuschner are passed through a 200 MHz bandpass filter centered on 1420 MHz and mixed with a local oscillator (LO) signal of frequency f_{LO}; both operations are performed at the antenna feed. The LO mixing sends frequencies of interest near 1420 MHz to intermediate frequencies ~ 150 MHz; this down-converted signal is routed to Leuschner Observatory facilities and bandpass filtered at 145–155 MHz.

We record an 8192 channel frequency spectrum with bandwidth 12 MHz centered on the intermediate frequency (IF) 150 MHz; spectral resolution is 1.5 kHz. Recall that IF frequencies correspond to radio frequencies $f - f_{\mathrm{LO}}$ (where f is radio sky frequency). The signal is digitized by an FPGA-based spectrometer using a polyphase filter bank; the effective sampling rate is 24 MHz. The signal of interest appears in our frequency output via Nyquist aliasing [*Siemion*, 2012].

For each point on the sky, we collect four raw spectra which are later reduced to a single calibrated spectrum. At a given LO frequency, we take two spectra: one with integration time 120 seconds, and one with integration time 12.5 seconds with a noise diode enabled. The noise diode injects power of a known temperature through the dish electronics, which permits us to convert spectrometer power to physical brightness temperature.

We take two spectra for each of two LO frequencies $f_{\rm LO} = 1268.9$ MHz and $f_{\rm LO} = 1271.9$ MHz; this enables frequency-dependent gain correction. The intermediate frequency range 144–156 MHz thus corresponds to the radio frequency bands 1412.9–1424.9 MHz and 1415.9–1427.9 MHz respectively.

2.2 Observing campaign

We observed the sky in the region $\{(l, b) \mid -150^\circ \leq l \leq 20^\circ, b \geq 0^\circ\}$, which contains the bulk of the North Polar Spur. Our observations were performed between 2014 April 26 to 2014 May 5. In order to completely map the sky, the region of interest should be sampled with angular spacing 2° (for beamwidth 4°); note that due to foreshortening, the spacing in galactic longitude is $2^\circ/\cos(b)$. Approximately 2500 pointings are required for complete sky coverage. Due to time constraints, we sampled most of the available region at 4° spacing in both galactic latitude/longitude.

Due to Leuschner's pointing limits, we are unable to collect data for a region roughly described by $\{(l, b) \mid -90^\circ \leq l \leq -20^\circ, 0^\circ \geq 38^\circ\}$. This blocks the base/stem of the spur, unfortunately, so we are limited to mapping the top and edges of the spur. From I. Domagalski's calculation, $\sim$ 940 points of our mapping region are never visible; we imaged $\sim$ 440 points and require $\sim$ 1100 more points for complete coverage of the remainder of the visible sky.

Our observations zig-zag along lines of fixed longitude during each observing window (nighttime $\sim$ 1600 to 0800 the next day), gradually incrementing in latitude from 0° to 90°. The status of ongoing observations may be monitored at http://ugastro.berkeley.edu/ domagalski/ay121/leuschner/status.html.

3 Data reduction

Our goal is to (1) convert unknown spectrometer intensity units to brightness temperature, and (2) remove the continuous bandpass filter

N.B. we may use the words power, intensity, and temperature interchangeably. Apologies for the technical imprecision... (I have not gone through and done the usual litany of checking that terms are defined at first usage and consistently used, not swapped out for synonyms). I don't think I've presented/explained our spectra usage well (i.e. sticking to a certain convention when explaining spectra).

3.1 Radio frequency interference

The radio spectrum from 1400 to 1427 MHz is internationally allocated for Earth exploration, space research, and radio astronomy (as of May 5, 2014). However, we observe radio frequency interference (RFI) at 1420 MHz. A 2001 RFI survey with the Rapid Prototype Array (RPA) near Leuschner Observatory [*Harp and Ackerman*, 2001] found no satellite RFI frequency near 1420 MHz; only the sun contributed significant interference. However, out-of-band signals from aeronautical radionavigation (960–1215 MHz) and telecommunications (various bands between 1350–1525 MHz) may also interfere with our observations. Since 2001, we expect that interference from communication signals should have increased substantially.

RFI appears as sharp power spikes in output frequency spectra. The quantity of interference spikes is highly variable (Figure 2). We did not explore how RFI may vary with altitude and azimuth or time of day.

We removed RFI spikes by binning spectra into bins of 4 channels and taking the bin channel with minimum power. We choose bin width 4 because our RFI spikes are typically localized to a single spectrometer channel, at most $2 - 3$ channels. Although ad hoc, this procedure empirically appears to work well.

3.2 Calibration

Prior to intensity calibration, we discard the 200 channels on each side of the spectra (without noise diode). The difference between spectra with and without noise should be proportional to noise diode temperature times frequency (channel) dependent gain. Figure 3 illustrates the effect of enabling noise diode.

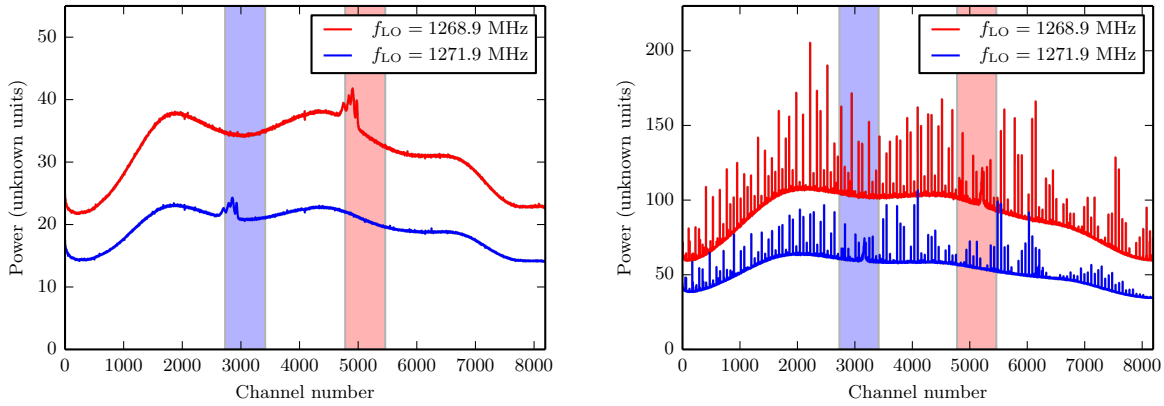

Figure 2. Raw spectra from each of two pointings show relatively low (left) and high (right) RFI. Channels correspond to different radio frequencies depending on f_{LO}, corresponding colored boxes for each LO frequency highlight the 1 MHz band centered on 1420.4 MHz. Note that spectra for different pointings have differing bandpass filter shapes and gains. Pointing coordinates are $l = 232.05°$, $b = 4°$ (left), $l = 16.01°$, $b = 20°$ (right). Raw spectra collected with noise diode for calibration are not shown but have comparable shapes, increased power offset, and increased noise.

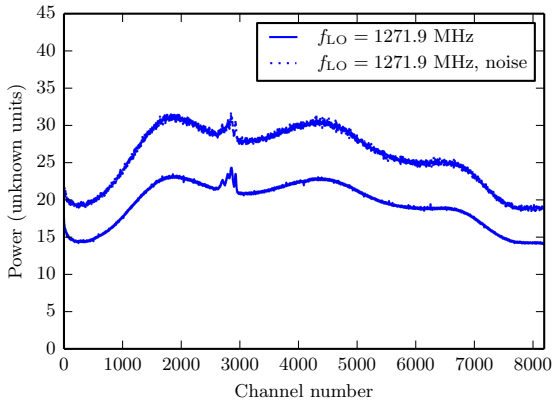

Figure 3. Spectra with (dots) and without (line) noise diode enabled. Same pointing as for left subplot of Figure 2.

To compare the system gain and temperature from multiple spectra, we need to remove the HI line. In all spectra we excise the region between 1419–1421.5 MHz (Figure 4) before processing.

For each set of spectra at a given f_{LO} we sum the channel-by-channel quotient between spectra with and without noise diode to estimate the gain effected by the noise diode. The noise diode adds $T \approx 100$ K and so we may calculate the gain

I wrote out the math for this procedure some time ago and it makes sense qualitatively, but Caleb's procedure is slightly different – it seems as if we compute the system temperature and gain separately for each set of spectra. Then, we use the un-noised data from each LO freq to subtract out the bandpass shape. Following this, the temperatures and frequencies are both averaged – though I'm not sure what the physical rationale for frequency averaging(?) is exactly. Refer to Caleb's report for a better account of the calibration procedure.

The output frequency range is 1419 to 1421.5 MHz

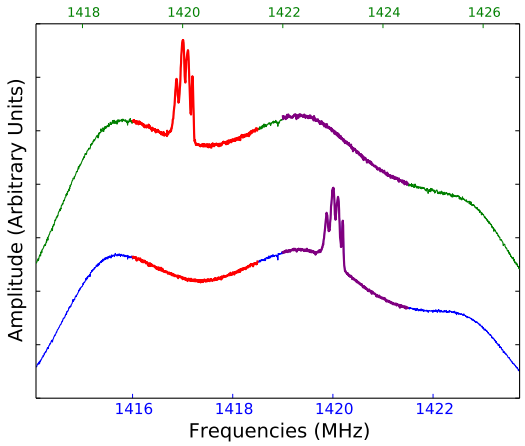

Figure 4. Excision procedure for system temperature and gain determination. Red, purple colors indicate region of the spectra that are removed in system temperature calculation. Same colors (i.e. spectral lines) are used to make a first pass at subtracting bandpass gain shape. Image is courtesy of C. Levy.

3.3 Error analysis

Integration times were chosen so error would be nice (mainly for noise). Integration time for main observations dictated by physical brightness temp. (mention that, when combining two measurements, error is minimized for balanced integration times) The following is copy pasted from our code pipeline's README, but I certify that I personally wrote this.

The (default) total integration time for both spectra is 87 * 2 * 0.692 sec/spec = 120 seconds. The (default) integration time for both noise spectra is 9 * 2 * 0.692 sec/spec = 12.5 seconds. Some earlier spectra were collected with doubled integration times. From prior experience (i.e., lab manual, suggestions in class, early test data etc), we choose 120 seconds to resolve features with T 1 to 10 K.

We desire that the calibration sum error be no more than 1/10th of error arising from individual channel uncertainty. The error of the noise calibration enters only through a sum term, so the error is scaled by 1/N where N is the number of channels summed. We conservatively take $N \sim 4096$ rather than 8192 (information lost from RFI removal, data cut at passband edges, etc.). Since the calibration integration time will be short, the calibration data is the main source of error in this sum. Looking at squared errors (as error scales with $1/\sqrt{(}$time)):

$$0.01 * \frac{1}{\text{integration time}} \sim \frac{1}{\text{calibration integration time}} * \frac{1}{4096}$$

The integration time with noise should be at least 0.02x the integration time of our actual data. Here the calibration integration time is 0.1x the integration time of our actual data. So we don't expect the calibration to contribute too much additional error.

However, as Caleb aggressively downsampled the data, this analysis may no longer be valid and the calibration noise error could contribute a non-trivial portion of observed error. The error analysis needs to be repeated.

4 Data analysis

4.1 Baseline removal and peak identification

Due to a shortage of time, I did not finish my own velocity computation etc scripts. Mainly needed baseline fitting/removal, peak identification. (but, after baseline removal, I'd be able to get the main science done).

Working on it now would require branching Isaac's pipeline, and risk messing up the current data processing pipeline. So I shan't do that yet...

Later on, I really want to be able to decompose the various peaks. It looks like our spur observations don't have multiple peaks anyways, so it's not so bad since we don't care about the galactic plane.

4.2 Useful quantities

I reproduce some comments from my code here.

From our finished spectra, with baselines removed and power scaled to brightness temperature, we calculate and generate plots of column density, mean velocity, and velocity standard deviation (a measure of dispersion)

The n-th moment of velocity, weighted by temperature/intensity $I(v)$, is:

$$E[v^n] = \left(\int v^n I(v) dv\right) / \left(\int I(v) dv\right)$$

The 0th moment is 1 (using normalization factor $\int I(v)dv$) and the 1st moment is the mean velocity v_{ave}.

The n-th *central* moment of velocity, weighted by temperature/intensity $I(v)$, is given by:

$$\mu_n = E\left[(v - v_{\text{ave}})^n\right] = \left(\int (v - v_{\text{ave}})^n I(v) dv\right) / \left(\int I(v) dv\right)$$

where v_{ave} is mean velocity as defined immediately prior. The 0th and 1st central moments are 1 and 0 respectively; the 2nd central moment is the velocity variance.

You may note that it is quite convenient to think of $I(v)$ as akin to an unnormalized probability density function (pdf); the normalized pdf is simply

$$\frac{I(v)}{\int I(v) dv}$$

where the integral is evaluated over $\mathbb{R}$. Our definitions of these moments correspond to those given by Wikipedia [en.wikipedia.org/wiki/Central_moment].

To calculate velocity standard deviation, we simply take the square root of the variance as usual.

4.3 Data interpolation and projection

I copped out and use matplotlib's griddata functionality, which performs a natural neighbor interpolation (n.b., distinct from *nearest* neighbor interpolation!) on irregularly spaced data points. I subsequently present contour maps of interpolated column density, mean velocity, and velocity standard deviation. Data projection is Mollweide equal-area.

5 Results

5.1 Maps of the North Polar Spur

Things to do:

- Manually compute Gaussian image interpolation
- Apply NaN mask to make imshow/contour/contourf plots better (instead of using a polygon to mask unmapped region). Maybe finish implementing signed distance function here to map out non-rectangular plot domain.

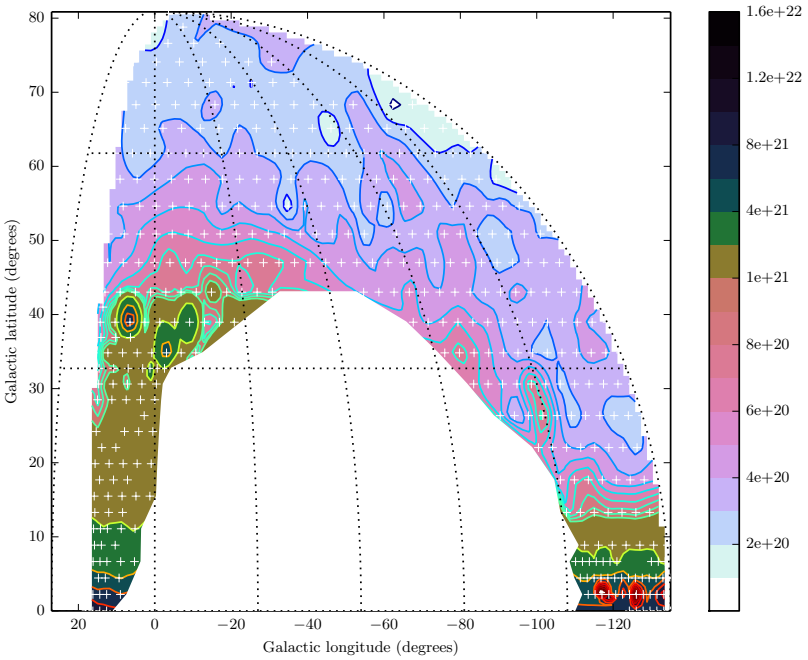

Figure 5. Column density. Units are cm^{-2}. Note that this is very roughly (i.e. manually) log scaled. Plot axis ticks are INCORRECT, though they have the generally correct trend. Gridlines are spaced 30° apart.

- Compare imshow/contour vs. contourf/contour. Imshow is continuous, technically carries more information.
- Consider conformal (stereographic), orthographic projections. Possibly include multiple images to replicate what a ground observer might see.
- Since we are not doing a complete sky map (which is what Mollweide is commonly used for), does there exist a more appropriate equal-area projection? Sinusoidal, Hammer, Aitoff, etc.
- Test colormaps in a systematic way. Determine physiologically sensible colormaps (i.e. no rainbows, jets)
- Determine best nonlinear colormapping for column density (logarithmic, power law). Maybe look at histogram and find the most "histogram-equalizing" transformation.
- Reduce the load times for both png and pdf... they're really slow. Maybe I should resort to jpg (welp, ugly, no)
- Multiple dimensions in color image – encode velocity (hue) and column density (brightness) together, with column density nonlinearly scaled.

5.2 Qualitative features

Comparing the dispersion to the velocity mean looks promising! As we might expect, dispersion is stronger towards the center of our postulated/expected bubble, a more robust velocity signal is seen at edges. However, these are very weak signals – our SNR gets smaller at high galactic latitudes, though the signal is quite evident still.

Give some example spectra, especially in that little spur of high dispersion.

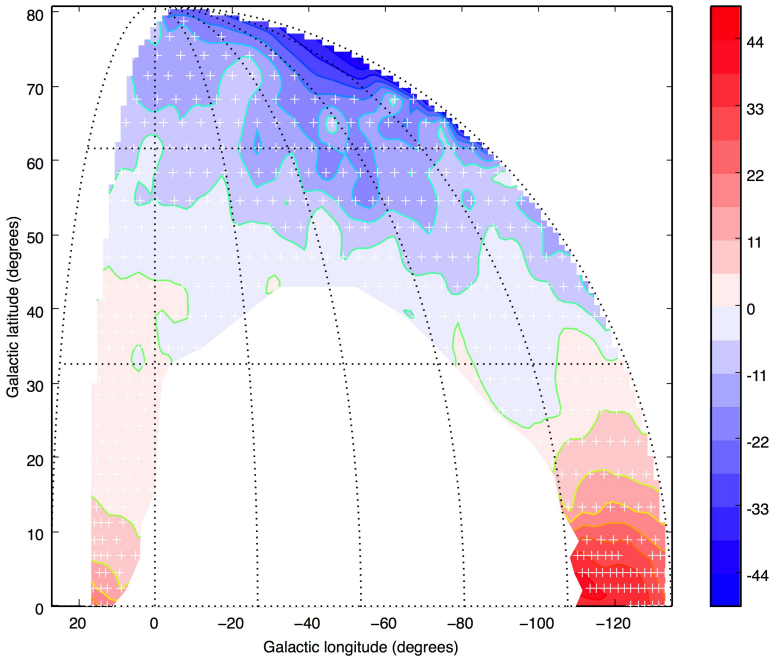

Figure 6. Mean velocity. Units are km/s. Same issues as in previous plots.

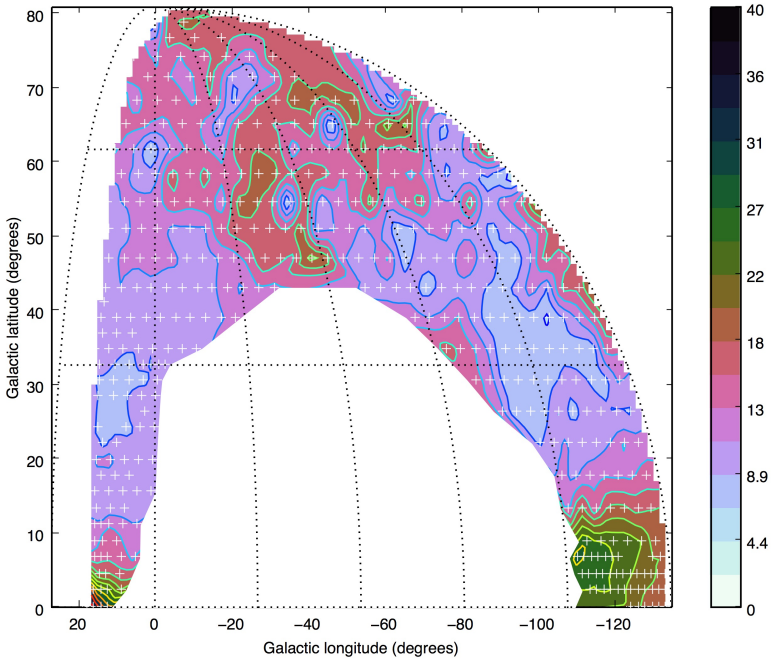

Figure 7. Std. dev. of velocity. Units are km/s. Same issues as in previous plots.

6 Discussion

6.1 Physical interpretation of observations

IF I separate out lines and get individual linewidths etc (by gaussian fit, dispersion for indiv peaks, however you like) – start considering physical phenomena that give rise to broadening.

Comparison, if there is time: download 1.4 GHz survey data from skyview.gsfc.nasa.gov and generate a comparison plot with same/similar projection.

6.2 Data reduction biases

RFI removal and calibration, and spectrum processing, naturally introduces biases. To remove RFI, we binned the frequency channels into groups of four and took the minimum value in each bin. Although this kills spikes, this also systematically biases our data downwards, particularly the channel readings where the HI line is present. We identify the selected bins with the ORIGINAL, ACTUAL frequency tied to that channel (so, the shape is roughly preserved, but the very peaks may be lost). We also introduce a more uneven frequency spacing and are throwing away data – this may increase error, although compared to the error of missing an RFI spike this may be a reasonable trade-off!

Caleb's procedure of throwing away 200 pts at edges of spectra – again, we are losing some (relatively unimportant) information. But, it helps cut down noise in the summation (more integration time, after a fashion).

6.3 RFI mitigation

Radio frequency interference was not actively characterized and addressed in this study. We suggest several approaches to addressing RFI in future work.

The quantity of interference signal is highly variable, with some spectra slathered in spikes and other spectra relatively unaffected. We speculate there may be multiple explanations. (1) geostationary satellites at fixed az-alt may contaminate certain pointings – this could be mitigated with prior knowledge of satellite az/alt. (2) airplanes. (3) if the RFI is from ground based transmission – e.g. if there are fewer transmissions at a certain time of day, or there is a directional dependence to broadcasts (wherever radio towers are located).

(if there is time – supply az,alt,time of pointings) (it would be nice to create a measure of how much RFI is present, then plot against az,alt to see if there is a portion of the sky that is particularly susceptible to contamination. We could do this with just our data for an incomplete, uneven survey, but it would be something.) (and, also plot the temporal dependance)

Tabulate list of sources https://casper.berkeley.edu/wiki/images/8/82/RPA5.pdf, see also VLA lists for examples.

Any future all-sky survey undertaken with the leuschner dish in May might want to map this region of the sky, then write the dish tracking script to avoid it. also keep track of where the sun and moon are.

If there is any way to probe polarization (as it seems they were once able to do with the RPA interferometer), we might be able to identify signals with strong polarization as being affiliated with human transmission [*Harp and Ackerman*, 2001].

7 Conclusions

Pretty pictures are gr8.

8 Appendix A: other colormaps

Comparison plots for different colormaps.

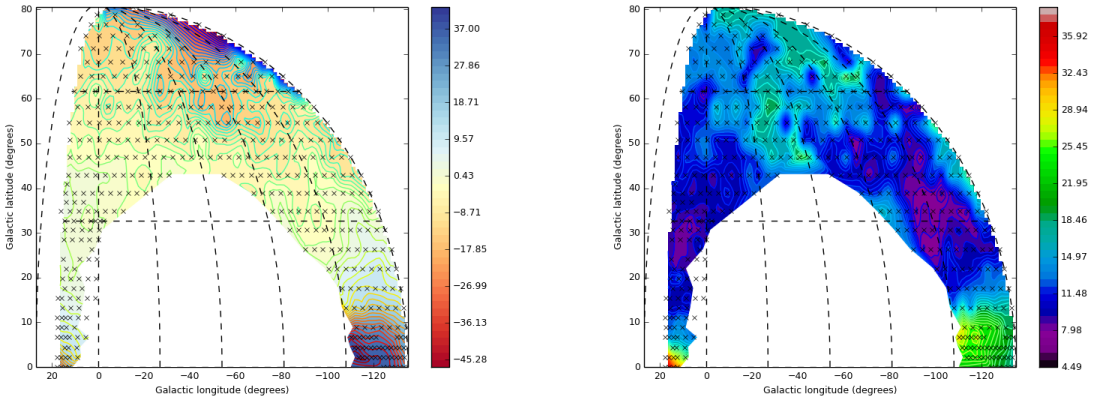

Figure 8. Mean velocity (left), stdev of velocity (right). Units are km/s for colors.

They look so pretty... but they're not as meaningful as they seem – see the arguments put forth by *Borland and Taylor II* [2007] in *Rainbow Color Map (Still) Considered Harmful*.

9 Acknowledgments

Kartp noster, qui es in radiolab:
sanctificetur nomen tuum;
adveniat regnum tuum;
fiat voluntas tua.
sicut in academia, et in universitas.
Observationem nostrum cotidianum da nobis hodie;
et dimitte nobis errores nostra,
sicut et nos dimittimus erroribus nostris;
et ne nos inducas in tentationem;
sed libera nos a circumsonum.

This lab was made possible by five pieces of duct tape (placed by Kartp noster).

10 Author contributions

I. A. D. did almost everything tracking. C. L. did all calibration. A. T. did some of the tracking. All parties contributed to debugging.

11 Electronic supplement

All supporting files are stored on the repository:
github.com/aarontran/ay121.

More thorough documentation and additional scripts/utilities may be found at: bitbucket.org/domagalski/cia-leuschner-pipeline/ and bitbucket.org/domagalski/astro121-radio-lab/ (the latter, in particular, has source for Isaac's status webpage at ugastro.berkeley.edu/ domagalski/ay121/leuschner/).

12 References

Borland, D. and R. M. Taylor II (2007), Rainbow color map (still) considered harmful, *27*(2), 14–17, doi:10.1109/MCG.2007.46.

Condon, J. J. and S. M. Ransom (2006), Essential Radio Astronomy, http://www.cv.nrao.edu/course/astr534/ERA.shtml.

Green, R. M. (1985), *Spherical astronomy*, 520pp., Cambridge Univ. Press, Cambridge.

Harp, G. R. and R. F. Ackermann (2001), RFI Survey at the RPA, https://casper.berkeley.edu/wiki/images/f/f9/RPA11.pdf.

Heiles, C., Y.-H. Chu, R. J. Reynolds, I. Yegingil, and T. H. Troland (1980), A new look at the North Polar Spur, *Astrophys. J.*, *242*, 533–540, doi:10.1086/158487.

Kleppner, D., H. M. Goldenberg, and N. F. Ramsey (1962), Properties of the hydrogen maser, *Appl. Optics*, *1*, 55–60, doi:10.1364/AO.1.000055.

Siemion, A. (2012), Leuschner Spectrometer, CASPER documentation wiki, https://casper.berkeley.edu/wiki/Leuschner_Spectrometer.

Wittke, J. P. and R. H. Dicke (1956), Redetermination of the hyperfine splitting in the ground state of atomic hydrogen, *Phys. Rev. Lett.*, *103*(3), 620–631, doi:10.1103/PhysRev.103.620.

Wolleben, M. (2007), A New Model for the Loop I (North Polar Spur) Region, *Astrophys. J.*, *664*, 349–356, doi:10.1086/518711.